PCCP

Nonlinear Electronic Excitation in Water under Proton Irradiation: A First Principles Study

Journal:	*Physical Chemistry Chemical Physics*
Manuscript ID	CP-ART-11-2021-005313.R2
Article Type:	Paper
Date Submitted by the Author:	08-Feb-2022
Complete List of Authors:	Shepard, Christopher; University of North Carolina at Chapel Hill College of Arts and Sciences, Chemistry Kanai, Yosuke; University of North Carolina at Chapel Hill College of Arts and Sciences, Chemistry

Nonlinear Electronic Excitation in Water under Proton Irradiation: A First Principles Study

Christopher Shepard and Yosuke Kanai
Department of Chemistry, University of North Carolina at Chapel Hill, NC, USA

Abstract

Nonlinear dynamics of electronic excitation bridge physical and physicochemical stages of water radiolysis under proton irradiation, a multi-scale physicochemical process that is fundamental to a wide range of technological and medical applications of high-energy protons. We study the spatial and temporal changes to the excited holes generated in this ionization event using first-principles theory simulation. A significant majority of holes are formed in the immediate vicinity of the irradiating proton paths, and these holes decay rapidly, while secondary excitations are simultaneously induced in regions farther away. While the hole population remains constant, the observed spatially spreading hole distribution cannot be described as concentration-dependent diffusion current. Compared to the primary excitation induced by the irradiating protons, the secondary excitation farther away is somewhat less energetic. The first-principles theory simulation here provides a detailed description of how the primary excitation by proton radiation precedes the formation of cationic holes, which undergo ultrafast chemical processes in water radiolysis.

1 Introduction

Water radiolysis is a physicochemical, multi-scale process, fundamental to various technological and biological phenomena when subjected to high-energy radiation. Ionization of liquid water leads to the formation of highly reactive species, particularly hydrated electrons and cationic holes on water molecules (i.e. H_2O^+). While the hydrated electron has been experimentally detected[2] and its dynamics have been studied extensively[3-8], the dynamics of the cationic hole specie was measured only recently by Loh, et al. using ultrafast X-ray spectroscopy in 2020.[9] In particular, they observed ultrafast chemical dynamics between cationic holes and water molecules, yielding OH radicals and hydronium cations, $H_2O^+ + H_2O \rightarrow OH\cdot + H_3O^+$, under 100 fs. This ultrafast dynamical process was further examined by first-principles Ehrenfest simulation which additionally showed not only the proton transfer, but also other related processes that can occur in such a short period of time.[10] Understanding these ultrafast processes represents a major advance in studies of water radiolysis. At the same time, we still lack understanding on how these ultrafast chemical dynamics depend on the radiation type. In the so-called physical stage of water radiolysis, the relevant dynamics is predominantly of electrons instead. In this temporal regime, the electron dynamics depend on the type of ionizing radiation (i.e. X-ray, γ-ray, charged particles) while it is usually assumed that excited electrons and holes have relaxed prior to the subsequent physicochemical stage. Although electronic excitation of water under electromagnetic irradiation like X/γ-ray has been widely studied, much less is known about the excitation under charged particle radiation. In particular, ion radiation, such as that of protons, has become quite important in recent years, especially from the viewpoint of developing detailed understanding of proton beam cancer therapy at the molecular level.[11] When an energetic ion travels through and interacts with condensed matter like water, its kinetic energy is transferred into the matter's electronic and nuclear subsystems. This energy loss by the irradiating ion can arise from both elastic collisions with nuclei (nuclear stopping) and inelastic scattering events (electronic stopping). When the particle's kinetic energy is sufficiently large (on the order of $\sim$10 keV per nucleon), electronic stopping is the primary energy transfer mechanism, wherein the irradiating ion induces massive electronic excitations in the target matter.[12, 13] In the context of water radiolysis, our recent first-principles theory works on electronic stopping have quantified the energy transfer rate (i.e. electronic stopping power) and the spatial characteristics of the induced electronic excitation.[14-16] At the same time, understanding on how the electronic excitation dynamics in proton

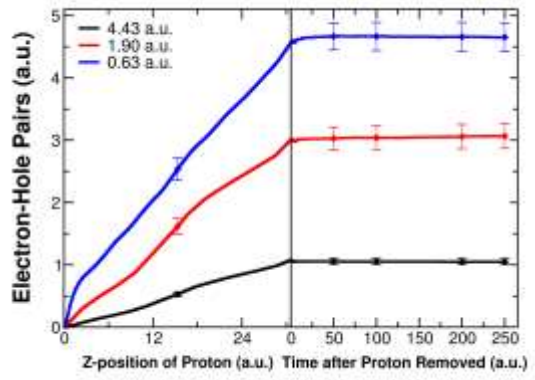

FIG.1. The number of electron-hole pairs (EHPs) averaged over an ensemble of 10 trajectories for each irradiating proton velocity. Once the irradiating proton reaches the end of the simulation cell and is removed from the simulation (marked t=0), the electronic states are propagated for an additional 250 a.u. (6.02 femtoseconds).

irradiation leads to the formation of cationic holes, which undergo ultrafast chemical dynamics, is missing. In this work, first-principles time-dependent simulation is used to study electron dynamics that immediately follow the primary excitation induced by proton irradiation. In particular, we focus on the non-linear electronic response to the electromagnetic field of the irradiating protons, following the initial excitation. The work here provides atomistic insights into the dynamics that bridge the physical and physicochemical stages of water radiolysis.

2 Computational Details

Following our earlier work on electronic stopping processes[14, 15, 17-19], real-time time-dependent density function theory (RT-TDDFT) is used to simulate non-perturbative excitation dynamics in liquid water under proton irradiation. We use our RT-TDDFT implementation based on the plane wave pseudopotential (PW-PP) formalism[20-22] in the Qbox/Qb@ll code.[23, 24] In the RT-TDDFT simulations, we express the single particle Kohn-Sham (KS) orbitals in the maximally localized Wannier function (MLWF)[25] gauge, rather than in the more commonly used Bloch representation. We propagate the time-dependent (TD) MLWFs[26] in the RT-TDDFT simulations. The structure of liquid water was generated by taking a snapshot of the equilibrated system following a 20 picosecond classical molecular dynamics simulation at 300 K using the single point charge with polarization correction (SPC/E) model.[27] A cubic simulation cell (16.229Å) containing 162 water molecules (1296 electrons) with periodic boundary conditions was used. Convergence of the simulated electronic excitation with respect to the water structure was checked by computing optical absorption spectra, and the water structure was examined against those from first-principles molecular dynamics and with respect to that of a larger simulation cell size (see Supplemental Material Fig. S1 and S2).[28] The generalized gradient approximation by Perdew-Burke-Ernzerhof (PBE)[33] was used for the exchange-correlation (XC) functional. GGA functionals, such as PBE, are known to give artificial charge delocalization in some cases.[34] However, previous work on liquid water has shown hybrid functionals such as PBE0 give nearly identical results to GGA:PBE when comparing projectile ion effective charge state and electronic stopping power.[15] Additional XC testing using recent meta-GGA:SCAN[35] is included in Supplemental Material S8. A plane wave cut-off energy of 50 Rydberg was used, along with Hamann-Schluter-Chiang-Vanderbilt (HSCV)[36, 37] norm-conserving pseudopotentials for all atoms. Γ-point-only sampling of Brillouin zone integration was sufficient for liquid water structure of this simulation size.[38] For all RT-TDDFT simulations, a 0.05 a.u. time step was used with the enforced time-reversal symmetry (ETRS) propagator.[39] The positions of all atoms, other than the irradiating (also called projectile) proton, were fixed, and only the electronic system was evolved in response to the time-dependent potential of the proton for the electronic stopping dynamics. Recent experimental work shows only small nuclear motions for neighboring waters over the first 10 fs even upon H_2O^+ formation in liquid water.[9] Given the relatively short simulation time of up to 7.25 fs for studying electron dynamics here, the nuclear motions are not considered in this work. Once the irradiating proton reached the end of the simulation cell, the proton was removed from the simulation,

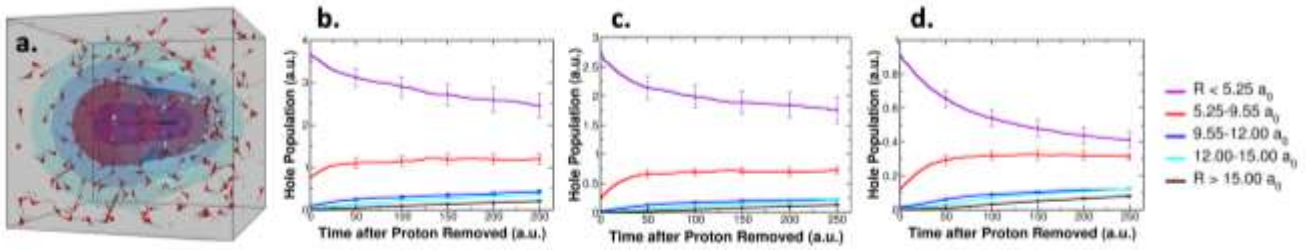

FIG. 2. (a) Five cylindrical "shell" regions surrounding the irradiating proton path. R < 5.25 a_0 (purple), 5.25-9.55 a_0 (red), 9.55-12.00 a_0 (blue), 12.00-15.00 a_0 (cyan), > 15.00 a_0 (black). The cylindrical shells are divided such that no wannier functions sit across the shell boundaries. (b-d) Hole population in each spatial region for different irradiating proton velocities. (b) 0.63a.u., (c) 1.90a.u., and (d) 4.43a.u.

and the simulation was propagated for an additional 6.02 fs. We also tested the use of a complex absorbing potential[40, 41] to remove the electron charge accumulated on the irradiating proton, but the results did not change as the localized charge on proton is quite small (see Fig. S3 in the Supplemental Material).[28] An ensemble of 10 randomly generated paths was sampled, with the irradiating proton traveling in the +*z* direction.

3 Results and Discussion

Figure 1 shows the number of generated electron-hole pairs (EHPs) in the simulation cell for the irradiating proton velocities of 0.63, 1.90, and 4.43 a.u., as a function of time after the proton is removed from the simulation. The number of EHPs was calculated by projecting the TD-MLWFs onto the equilibrium KS eigenstates in the valence band and quantifying the time-dependent changes in their occupations. The velocities were chosen based on stopping power calculated in previous works.[14, 15] Figure 1 shows that the proton velocity of 0.63 a.u. results in the most significant EHP increase, not the stopping power maximum velocity of 1.90 a.u. Such a difference between the velocities for the maximum EHPs and for the stopping power maximum has been observed also for DNA.[16] This is not necessarily surprising because large stopping power (i.e. energy transfer rate) could result from the excitation of electrons from electronic states that are comparatively deep in energy. We also note that the proton velocities of 0.63 a.u. and 4.43 a.u. yield similar stopping powers[14] despite the significant difference in the EHPs. Once the irradiating proton reaches the end of the simulation cell and is removed from the simulation (*t*=0 in Figure 1), no work is done on the system and the number of EHPs remains essentially constant for all velocities. Electronic excitation under ionizing irradiation can be of neutral excitation or more of ionization in character.[42, 43] In order to quantify this aspect, the TD-MLWFs are projected onto a set of unoccupied (i.e. conduction band) KS eigenstates that covers 10.75 eV above the conduction band minimum (CBM). This energy range essentially covers all the conduction band states up to the vacuum level[44], and transitions of electrons into the electronic states above this energy manifold can be considered ionization. For the 4.43 a.u. and 1.90 a.u. velocities, the excitations are largely ionization in character, as less than 25% of the excited electrons are found to be below this ionization threshold at any instance of time (see Fig. S4 in the Supplemental Material).[28] For the lowest proton velocity of 0.63 a.u., the excitations are noticeably less ionizing, with more than 40% of the excited electrons below this energy threshold.

Excited electrons that are generated in ionization events by the primary radiation (e.g. irradiating protons) are often referred to as secondary electrons, and they have a relatively short mean free path of 1~10 nm for the relevant energy range.[45] A large body of literature exists on the secondary electrons[46-49], and they are usually treated as the secondary radiation, being distinguished from the primary radiation. In the context of electronic stopping excitation in water, the majority of excited electrons are highly itinerant, even those below the vacuum level.[14, 50] These secondary electrons are the likely source of hydrated electrons, which are formed on a longer timescale into pico-seconds.[7, 51-54] At the same time, dynamics of the generated holes have not been investigated to the same extent. Recent experimental work showed that the cationic hole, H_2O^+, undergoes an ultrafast chemical reaction to form OH radicals within 100 fs[9], and first-principles Ehrenfest dynamics work also revealed other equally rapid processes.[10] In electronic stopping, electrons are excited away from the immediate vicinity of the irradiating proton paths,

generating highly-localized concentrations of holes.[14] Thus, the distribution of H_2O^+ species in water would depend on the spatial and temporal changes of the generated holes by the proton radiation, making this consideration particularly important given such ultrafast processes H_2O^+ undergoes. In order to investigate dynamics of the hole generation, we examine non-linear effects in our RT-TDDFT simulation by analyzing spatial and time dependent changes of TD-MLWFs. The TD-MLWFs are localized on individual water molecules even in liquid, and the hole population can be decomposed into different spatial regions, defined by distance from the center of proton paths. As shown in Fig. 2(a), we define five spatial regions using cylindrical shells. Averaged hole population (per water molecule) in each cylindrical shell, *S*, is quantified by

$$HP_s(t) = \frac{1}{N_s}\sum_{I\in s}^{N_s}\sum_{i}^{4}\sum_{j}^{n}\left(2 - \left|\langle\psi_j|w_i^I(t)\rangle\right|^2\right) \quad (1)$$

where N_s is the number of molecules in each shell. Each TD-MLWF, $|w_i^I(t)\rangle$, can be identified with individual water molecules, *I*, and four TD-MLWFs (two for lone-pair electrons and two for OH bonds) are identified for each water molecule. $|\psi_j\rangle$ are the occupied (i.e. valence band) eigenstates of the equilibrium system, and the nuclei are not moved in the simulations. The regions for each cylindrical shell *S* are defined such that no Wannier centers (the expectation value of the position operator[39]) reside on the boundaries. As the irradiating proton moves through water, over 80% of the holes are generated within 5.25 Bohr (a_0) of the paths. While the total hole population remains nearly constant after the irradiating proton is removed from simulation at *t*=0, an immediate decay of the holes is observed near the proton track and simultaneous excitations in the regions farther away from the proton paths. Figure 2 (b-d) shows the hole population changes in different spatial regions as a function of time for the three irradiating proton velocities. The decay of holes is observed only in the region closest to the proton paths, while the hole population growths show up in other regions to varying degrees. These secondary excitations are evident even in the most distant region, and they are observed for all velocities considered here. In the closest region to the irradiating proton paths (i.e. R < 5.25 a_0), more than 30% of the holes decay within 250 a.u. (6.02 fs). Concurrently, other regions show a more gradual increase in the hole population. By 6 fs, more than 10% of the total hole population is in the two farthest regions from the irradiating proton paths (i.e. R > 12.00 a_0). The rates with which the hole population changes vary in time initially, but they approach a plateau value on a relatively short time scale within t=75 a.u (2.9 fs) (Fig. S5 in the Supplemental Material).[28] In the two regions farthest from the paths, the hole population change is always positive and shows a nearly constant average.

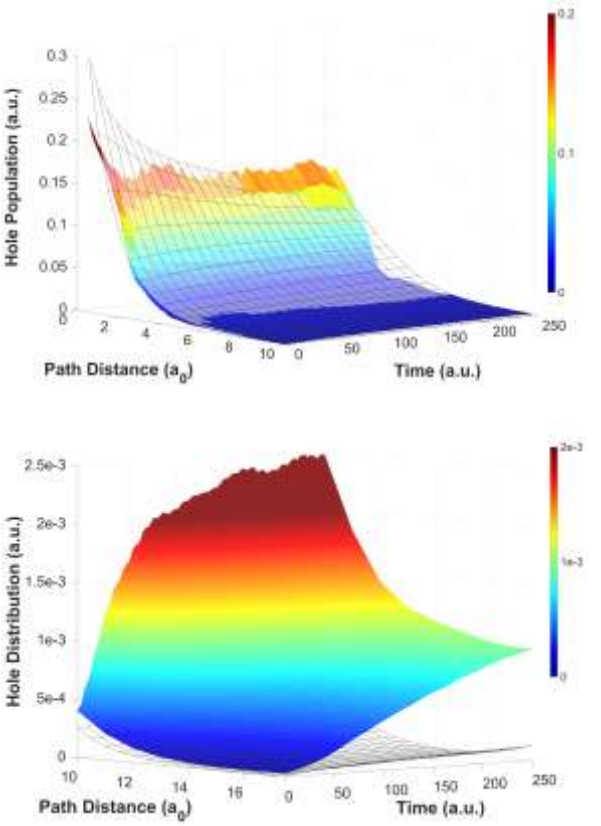

FIG.3 Temporally and spatially dependent hole distributions in water, overlaid with diffusion model (shown as a dark mesh) in (top panel) R < 10 a_0 and (bottom panel) R > 10 a_0. A Savitzky-Golay filter[1] is used in order for the first-principles simulation data to be fit to the diffusion model.

Particle current due to a non-uniform concentration of holes is often viewed as diffusion current in condensed matter physics, in contrast to drift current which is caused by an external electric field such as that from irradiating protons. We examine the extent to which the observed behavior of spatially-spreading holes (while the total hole

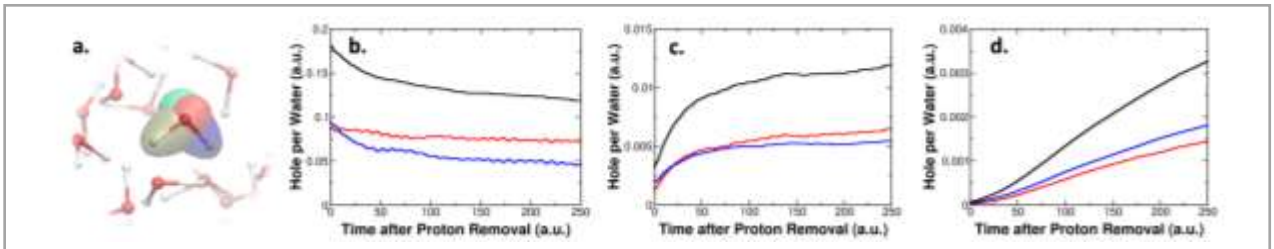

FIG.4(a) Maximally localized Wannier functions for a single water in liquid water. (b-d) Changes in hole population for the 1.90 a.u. velocity, decomposed into contributions from lone-pair holes and O-H bond holes for (a) R < 5.25 a_0. (b) R=5.25-15.00 a_0. (c) R > 15.00. Black line represents total hole populations changes per water, while blue and red represent the contributions from lone-pair and OH bond centered TD-MLWFs, respectively.

population remains essentially constant) can be described as such semi-classical diffusion current. We employ a cylindrical diffusion model in which the holes diffuse in the radial direction[55],

$$\frac{\partial C(R,t)}{\partial t} = \frac{1}{R}\frac{\partial}{\partial R}\left(R \times D\frac{\partial C(R,t)}{\partial R}\right) \quad (2)$$

where the concentration $C(R,t)$ is taken as the hole distribution and R is the radial distance from the center of the proton paths. D is the diffusion constant. To obtain a continuous function for performing an analytical fit to the diffusion model (the least squares fitting), the RT-TDDFT simulation data is pre-processed with Savitzky-Golay filter.[1] Fig. 3 shows that the classical diffusion model with the best fit value of $D = 7 \times 10^{-3}\ holes/(a.u.(time)^2 \times a_0)$ and also the first-principles simulation result for the proton velocity of 1.90 a.u. Two key differences between the diffusion model and the simulation results are observed. First, the decay rate near the irradiating proton paths is much more gradual in the diffusion model while the actual hole decay is better described as an exponential decay. Secondly, the growth in the distant regions is much slower in the diffusion model. These observations are rather insensitive to the specific diffusion constant value D, and the same conclusion holds also for the 0.63 a.u. and 4.43 a.u. velocities but with slightly larger diffusion constants of $1.1 \times 10^{-2}\ holes/(a.u \times a_0)$ and $1.3 \times 10^{-2}\ holes/(a.u.(time)^2 \times a_0)$, respectively (Fig. S8-S9 of the Supplemental Material).[28]

The dynamics of the holes can be further analyzed from the perspective of chemical moieties. On individual water molecules, two sets of the TD-MLWFs can be identified; one for lone-pair electrons and one for OH covalent bonds as shown in Fig. 4(a).[56] Lone-pair electron orbitals and OH bonds electron orbitals contribute near equally to the initial excitation. However, as seen in Fig. 4(b) for the velocity of 1.90 a.u., the decay of holes near the irradiating proton paths (R<5.25 a_0) is primarily due to the lone-pair electron orbitals. For the 1.90 and 0.63 a.u. velocities, 76% and 78% of the decay is attributed to the lone pairs, respectively. The 4.43 a.u. velocity shows a slightly smaller contribution, with 62% of the hole decay coming from the lone pairs. Both lone-pair electron orbitals and OH bond orbitals are equally responsible for the hole population growths from the secondary excitation in the outer regions, as seen in Fig. 4(c-d). As expected from this observation, energetics of the holes is somewhat different for those that are

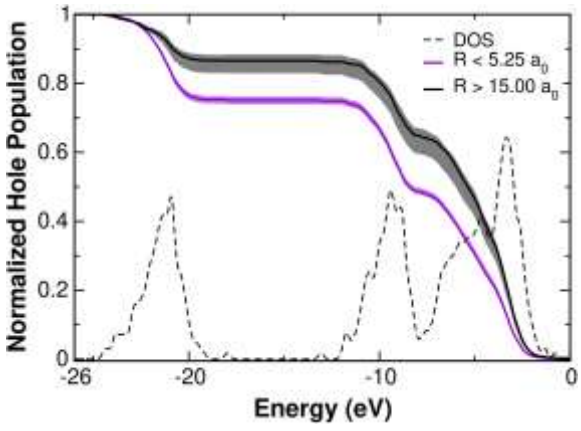

FIG.5. Cumulative hole population integrated from the VBM (E=0 eV) for the primary excitation in R < 5.25 a_0 at t=0 and for the secondary excitation in R > 15 a_0 at t=250 a.u. for the 1.9 a.u. velocity (solid lines). The shaded regions below each curve represents the 4.43. a.u. velocity and the shaded regions above represents the 0.63 a.u. velocity. Density of states is shown as a reference.

generated in the secondary excitations farther away from the irradiating proton paths. Fig. 5 shows the cumulative hole population from the primary excitation in the closest region ($R<5.25\ a_0$) and from the secondary excitation in the farthest region ($R>15.00\ a_0$). The hole population is integrated from the valence band maximum (VBM) to lower energies. All holes are generated within 26 eV of the VBM. In general, the more distant from the irradiating proton paths, the larger percentage of the holes are formed close the VBM; the secondary excitations generate holes that are less energetic than those generated in the primary excitation by the irradiating protons. In the primary excitation, approximately half the holes are formed within 8 eV of the VBM, which corresponds to the most prominent peak in the density of states. We find essentially no dependence on the proton projectile velocity. In the secondary excitation, a larger percentage of holes are formed within 8 eV of the VBM; 60%, 60% and 67% in the farthest region (i.e. $R>15.00\ a_0$) for the velocity of 4.43 a.u., 1.90 a.u., and 0.63 a.u., respectively.

4 Conclusion

The nonlinear electronic response in water is fundamental to understating water radiolysis under high energy proton irradiation. Employing first-principles simulation, we studied the spatial and temporal dependence of the dynamics of holes generated in water under proton irradiation. A significant majority of holes are generated in the immediate vicinity of the irradiating proton paths. The simulation revealed that the holes decay rapidly while secondary excitations are simultaneously induced in regions farther away from the irradiating proton paths. The semi-classical diffusion current model does not adequately describe this spatially spreading hole distribution while the hole population remains essentially constant. Lone-pair electron orbitals are primarily responsible for the hole decay while OH bond-centered electron and lone-pair electron orbitals equally contribute to the secondary excitation farther away. Compared to the primary excitation induced by the protons, the secondary excitation is somewhat less energetic. A greater percentage of holes are formed near the VBM in the secondary excitation. Our first-principles theory simulation of nonlinear excitation dynamics in water under proton irradiation here provides a quantum-mechanical description of how the primary excitation by proton radiation precedes the formation of cationic holes, which undergo sub-100fs chemical processes in water radiolysis. While including nuclear motion within RT-TDDFT is possible at the level of Ehrenfest dynamics, the quantum nature of protons in water might complicate simulations of coupled electron-nuclear dynamics necessary for investigating excitation-induced dissociation of water molecules.[57, 58] Future work will address this great challenge with developing advanced methodologies.

Conflicts of Interest

There are no conflicts to declare.

Acknowledgement

An award of computer time was also provided by the Innovative and Novel Computational Impact on Theory and Experiment (INCITE) program. This research used resources of the Argonne Leadership Computing Facility (ALCF), which is a DOE Office of Science User Facility supported under Contract No. DE-AC02-06CH11357.

References

1. A. Savitzky and M. J. E. Golay, *Analytical Chemistry*, 1964, **36**, 1627-1639.
2. E. J. Hart and J. W. Boag, *Journal of the American Chemical Society*, 1962, **84**, 4090-4095.
3. A. Migus, Y. Gauduel, J. L. Martin and A. Antonetti, *Physical Review Letters*, 1987, **58**, 1559-1562.
4. C. Silva, P. K. Walhout, K. Yokoyama and P. F. Barbara, *Physical Review Letters*, 1998, **80**, 1086-1089.
5. M. Assel, R. Laenen and A. Laubereau, *The Journal of Chemical Physics*, 1999, **111**, 6869-6874.
6. K. R. Siefermann, Y. Liu, E. Lugovoy, O. Link, M. Faubel, U. Buck, B. Winter and B. Abel, *Nature Chemistry*, 2010, **2**, 274-279.

7. R. E. Larsen, W. J. Glover and B. J. Schwartz, *Science*, 2010, **329**, 65-69.
8. J. M. Herbert, *Physical Chemistry Chemical Physics*, 2019, **21**, 20538-20565.
9. Z.-H. Loh, G. Doumy, C. Arnold, L. Kjellsson, S. H. Southworth, A. A. Haddad, Y. Kumagai, M.-F. Tu, P. J. Ho, A. M. March, R. D. Schaller, M. S. B. M. Yusof, T. Debnath, M. Simon, R. Welsch, L. Inhester, K. Khalili, K. Nanda, A. I. Krylov, S. Moeller, G. Coslovich, J. Koralek, M. P. Minitti, W. F. Schlotter, J.-E. Rubensson, R. Santra and L. Young, *Science*, 2020, **367**, 179-182.
10. L. Lu, A. Wildman, A. J. Jenkins, L. Young, A. E. Clark and X. Li, *J. Phys. Chem. Letters*, 2020, **11**, 9946-9951.
11. R. Alan Mitteer, Y. Wang, J. Shah, S. Gordon, M. Fager, P.-P. Butter, H. Jun Kim, C. Guardiola-Salmeron, A. Carabe-Fernandez and Y. Fan, *Scientific Reports*, 2015, **5**, 13961.
12. C. P. Race, D. R. Mason, M. W. Finnis, W. M. C. Foulkes, A. P. Horsfield and A. P. Sutton, *Rep. Prog. Phys.*, 2010, **73**, 116501.
13. J. F. Ziegler, *J. Appl. Phys.* , 1999, **85**, 1249-1272.
14. Y. Yao, D. C. Yost and Y. Kanai, *Physical Review Letters*, 2019, **123**, 066401.
15. K. G. Reeves, Y. Yao and Y. Kanai, *Phys. Rev. B*, 2016, **94**, 041108.
16. D. C. Yost and Y. Kanai, *Journal of the American Chemical Society*, 2019, **141**, 5241-5251.
17. K. G. Reeves and Y. Kanai, *Sci Rep*, 2017, **7**, 40379.
18. D. C. Yost and Y. Kanai, *Phys. Rev. B*, 2016, **94**, 115107.
19. D. C. Yost, Y. Yao and Y. Kanai, *Phys. Rev. B*, 2017, **96**, 115134.
20. A. Schleife, E. W. Draeger, V. M. Anisimov, A. A. Correa and Y. Kanai, *Comput. Sci. Eng.*, 2014, **16**, 54-60.
21. A. Schleife, E. W. Draeger, Y. Kanai and A. A. Correa, *J. Chem. Phys.*, 2012, **137**, 22A546.
22. C. Shepard, R. Zhou, D. C. Yost, Y. Yao and Y. Kanai, *The Journal of Chemical Physics*, 2021, **155**, 100901.
23. F. Gygi, *IBM Journal of Research and Development*, 2008, **52**, 137-144.
24. F. Gygi, *Lawerence Livermore National Laboratory*.
25. N. Marzari and D. Vanderbilt, *Phys. Rev. B*, 1997, **56**, 12847-12865.
26. F. Gygi, J.-L. Fattebert and E. Schwegler, *Comput. Phys. Commun.*, 2003, **155**, 1-6.
27. H. J. C. Berendsen, J. R. Grigera and T. P. Straatsma, *J. Phys. Chem.*, 1987, **91**, 6269-6271.
28. See Supplemental Material for computational and diffision model details and comparisons to other velocities.
29. C. A. Ullrich, *Time-dependent density-functional theory : concepts and applications*, Oxford University Press2006.
30. D. C. Yost, Y. Yao and Y. Kanai, *The Journal of Chemical Physics*, 2019, **150**, 194113.
31. C. Fonseca Guerra, J.-W. Handgraaf, E. J. Baerends and F. M. Bickelhaupt, *Journal of Computational Chemistry*, 2004, **25**, 189-210.
32. C.-k. Li, F. Mao, F. Wang, Y.-l. Fu, X.-p. Ouyang and F.-S. Zhang, *Physical Review A*, 2017, **95**, 052706.
33. J. P. Perdew, K. Burke and M. Ernzerhof, *Physical Review Letters*, 1996, **77**, 3865-3868.
34. A. J. Cohen, P. Mori-Sánchez and W. Yang, *Science*, 2008, **321**, 792-794.
35. J. Sun, A. Ruzsinszky and J. P. Perdew, *Physical Review Letters*, 2015, **115**, 036402.
36. D. R. Hamann, M. Schlüter and C. Chiang, *Physical Review Letters*, 1979, **43**, 1494-1497.
37. D. Vanderbilt, *Phys. Rev. B*, 1985, **32**, 8412-8415.
38. D. Prendergast, J. C. Grossman and G. Galli, *J. Chem. Phys.*, 2005, **123**, 014501.
39. A. Castro, M. A. L. Marques, J. A. Alonso, G. F. Bertsch and A. Rubio, *Eur. Phys. J. D*, 2004, **28**, 211-218.
40. T. Nakatsukasa and K. Yabana, *J. Chem. Phys.*, 2001, **114**, 2550-2561.
41. T. Otobe, K. Yabana and J. I. Iwata, *Phys. Rev. A*, 2004, **69**, 053404.
42. M. A. Huels, B. Boudaïffa, P. Cloutier, D. Hunting and L. Sanche, *Journal of the American Chemical Society*, 2003, **125**, 4467-4477.
43. R. H. Eather, *Journal of Geophysical Research (1896-1977)*, 1966, **71**, 4133-4140.
44. C. F. Perry, P. Zhang, F. B. Nunes, I. Jordan, A. von Conta and H. J. Wörner, *J. Phys. Chem. Letters*, 2020, **11**, 1789-1794.
45. H. Nikjoo, S. Uehara, D. Emfietzoglou and A. Brahme, *New J. Phys.*, 2008, **10**, 075006.
46. Y.-K. Kim, *Radiation Research*, 1975, **61**, 21-35.
47. Mehnaz, L. H. Yang, Y. B. Zou, B. Da, S. F. Mao, H. M. Li, Y. F. Zhao and Z. J. Ding, *Medical Physics*, 2020, **47**, 759-771.
48. D. A. Vroom and R. L. Palmer, *The Journal of Chemical Physics*, 1977, **66**, 3720-3723.
49. D. Emfietzoglou, G. Papamichael and M. Moscovitch, *Journal of Physics D: Applied Physics*, 2000, **33**, 932-944.

50. E. Scifoni, E. Surdutovich and A. V. Solov'yov, *Phys. Rev. E*, 2010, **81**, 021903.
51. J. M. Herbert and M. P. Coons, *Annual Review of Physical Chemistry*, 2017, **68**, 447-472.
52. V. Cobut, Y. Frongillo, J. Patau, T. Goulet, M. Fraser and J. Jay-Gerin, *Radiation Physics and Chemistry*, 1998, **51**, 229-243.
53. S. Uehara and H. Nikjoo, *Journal of radiation research*, 2006, **47 1**, 69-81.
54. C.-C. Zho, E. P. Farr, W. J. Glover and B. J. Schwartz, *The Journal of Chemical Physics*, 2017, **147**, 074503.
55. J. Crank, *The Mathematics of Diffusion*, Clarendon Press, Oxford [England], 1975.
56. K. G. Reeves and Y. Kanai, *Scientific Reports*, 2017, **7**, 40379.
57. I. Tavernelli, M.-P. Gaigeot, R. Vuilleumier, C. Stia, M.-A. Hervé du Penhoat and M.-F. Politis, *ChemPhysChem*, 2008, **9**, 2099-2103.
58. M. P. Gaigeot, R. Vuilleumier, C. Stia, M. E. Galassi, R. Rivarola, B. Gervais and M. F. Politis, *Journal of Physics B: Atomic, Molecular and Optical Physics*, 2006, **40**, 1-12.